A Heat Transfer Model Based on Finite Difference Method for Grinding

Bin Shen[1]

Albert J. Shih

Department of Mechanical Engineering,
University of Michigan,
Ann Arbor, MI 48109

Guoxian Xiao

Manufacturing Systems Research Lab,
General Motors R&D,
Warren, MI 48092

A heat transfer model for grinding has been developed based on the finite difference method (FDM). The proposed model can solve transient heat transfer problems in grinding, and has the flexibility to deal with different boundary conditions. The model is first validated by comparing it with the traditional heat transfer model for grinding which assumes the semiinfinite workpiece size and adiabatic boundary conditions. Then it was used to investigate the effects of workpiece size, feed rate, and cooling boundary conditions. Simulation results show that when the workpiece is short or the feed rate is low, transient heat transfer becomes more dominant during grinding. Results also show that cooling in the grinding contact zone has much more significant impact on the reduction of workpiece temperature than that in the leading edge or trailing edge. The model is further applied to investigate the convection heat transfer at the workpiece surface in wet and minimum quantity lubrication (MQL) grinding. Based on the assumption of linearly varying convection heat transfer coefficient in the grinding contact zone, FDM model is able to calculate convection coefficient from the experimentally measured grinding temperature profile. The average convection heat transfer coefficient in the grinding contact zone was estimated as 4.2×10^5 *W/m*^{2}*-K for wet grinding and* 2.5×10^4 *W/m*^{2}*-K for MQL grinding using vitrified bond CBN wheels.* [DOI: 10.1115/1.4003947]

1 Introduction

The energy required to remove a unit volume of work-material for grinding is very high. Virtually all this energy is converted to heat, which can cause high temperatures and thermal damage to the workpiece such as grinding burn, phase transformations, undesirable residual tensile stresses, cracks, reduced fatigue strength, thermal distortion, and inaccuracies [1]. Workpiece thermal damage is the major limitation to increase the material removal rate in grinding.

A considerable research effort has been devoted to both theoretical and experimental aspects of heat transfer in grinding. The classic thermal analysis of moving heat source and the temperature at sliding contacts was studied by Jaeger [2]. The application of Jaeger's moving heat source solutions to heat transfer problems in grinding was first proposed by Outwater and Shaw [3], whereby the grinding contact zone is approximated as a heat source moving along the surface of the workpiece. Outwater and Shaw [3] assumed that grinding heat is mainly generated at the shear plane, and thus the grinding temperature can be calculated by matching the average temperatures on the shear plane. Hahn [4] considered the frictional rubbing forces on the clearance surface and neglected cutting forces on the rake surface in the model. Snoeys et al. [5] and Malkin [6] both presented a comprehensive literature review of early research work on the prediction of workpiece surface temperatures in dry grinding without significant convective heat transfer.

Takazawa [7] considered the partitioning of energy over the grinding contact zone based on the grinding wheel bulk thermal properties. Similar contact zone thermal model was also proposed by Rowe et al. [8]. Shaw [9] considered both real and apparent contact areas, and used an area ratio factor to correlate grain properties with such a model.

Hahn [10,11] developed the heat transfer model for grinding based on the microscale thermal transport phenomenon at the grain-workpiece interface. Several other grain scale grinding heat transfer models have been developed [12–14]. Lavine [15] combined the grain-scale or microscale and wheel/workpiece macroscale thermal analysis for grinding. The wheel and grinding fluid were considered to be a composite solid moving at the wheel speed. It predicted the convective heat transfer coefficient on the workpiece surface, the fraction of energy entering the workpiece, and the workpiece surface temperature. In the following research work by Lavine and Jen [16,17], the heat transfer into abrasive grain, grinding fluid and workpiece are modeled separated by introducing local heat transfer coefficients, and the separate models are coupled by matching the temperature at the workpiece-fluid interface and the workpiece-grain interface. The model was further extended to account for the variation of the heat fluxes along the grinding contact zone in down grinding with large Peclet number [18]. Later a similar thermal model for up grinding [19] was developed to compare the workpiece temperature rises in up grinding and down grinding, and to explore the effect of the location of heat generation. Ju et al. [20] developed a comprehensive heat transfer model for grinding that covers both up surface grinding and down surface grinding without the assumption of large Peclet number. Lavine's model [18,19] differs from Ju's [20] in how the shear plane and grain geometry are modeled, and the assumption that if there is conduction in the direction of motion in the workpiece.

Temperature measurements in the workpiece subsurface during grinding indicated that the triangular heat source is more accurate than the rectangular one [21]. Analytical investigations by Guo and Malkin [22] indicated that energy partition (ratio of the energy entering the workpiece) is approximately constant along the grinding contact zone for regular down grinding, but varies greatly along the grinding contact zone for regular up grinding and both up creep-feed grinding and down creep-feed grinding.

Based on the measured surface temperature, the inverse heat transfer method was first applied by Guo and Malkin [23,24] to estimate the heat flux and local convective heat transfer coefficient on the workpiece surface. Inverse heat transfer models have been further studied extensively in grinding processes [25–27].

[1]Dr. Shen currently works for Procter & Gamble (Gillette Blades & Razors).

Contributed by the Manufacturing Engineering Division of ASME for publication in the JOURNAL OF MANUFACTURING SCIENCE AND ENGINEERING. Manuscript received October 2, 2009; final manuscript received March 4, 2011; published online June 2, 2011. Assoc. Editor: Shreyes N. Melkote.

Copyright © 2011 by ASME

Downloaded 07 Aug 2011 to 141.212.213.57. Redistribution subject to ASME license or copyright; see http://www.asme.org/terms/Terms_Use.cfm

Most of the thermal models for grinding have assumptions such as the steady-state condition, semi-infinite workpiece size, and adiabatic boundary condition (except for the heat flux in the grinding contact zone) on the workpiece surface. Both the finite element method (FEM) and the finite difference method (FDM) can overcome these constraints. Guo and Malkin [28] has developed a FDM based heat transfer model for grinding to study the transient grinding temperature and shown that the workpiece temperature rises rapidly during the initial wheel-workpiece engagement, subsequently reaches a quasi-steady state value if the workpiece is sufficiently long, and further increases in the final wheel-workpiece disengagement. The FEM has been applied to simulate the workpiece grinding temperature and analyze the phase transformation and thermal stress on ground surface [29–33].

In this study, a heat transfer model based on the FDM is developed to study the thermal aspects in grinding. In addition to the transient heat transfer problem as Guo and Malkin [28] has already studied, the main goal of this study is to investigate the convection heat transfer boundary conditions. More accurate convection heat transfer information can improve the prediction of grinding temperature (background temperature). The FDM heat transfer model is introduced in Sec. 2 and validated by comparing with the solution of the traditional heat transfer model in Sec. 3. Effects of workpiece dimension, feed rate, and cooling boundary conditions are studied using the FDM heat transfer model in Secs. 4 and 5. In Sec. 6, the FDM heat transfer model is further applied in the grinding experiment to estimate the energy partition and convection heat transfer coefficient.

2 Finite Difference Heat Transfer Model

In FDM the computation domain is subdivided into small regions and each region is assigned a reference point. In this study, the computation domain is the workpiece, as shown in Fig. 1(*a*). The node is at the center of the region, and designated by indices (m,n), as seen in Fig. 1(*b*). The grid size is defined as the distance between the two adjacent nodes. In this study, the uniform grid size is used, i.e., $\Delta x = \Delta z$. The moving heat source is assumed to be triangular.

2.1 Governing Equation. The computation domain is characterized in terms of a nodal network. The governing equation and boundary conditions can be transformed to the finite difference form. The 2D heat transfer governing equation is:

$$\frac{\partial^2 T}{\partial x^2} + \frac{\partial^2 T}{\partial z^2} = \frac{1}{\alpha}\frac{\partial T}{\partial t} \tag{1}$$

where α is the thermal diffusivity of the workpiece. Using the finite difference discretization, Eq. (1) for the nodes (m,n) (as shown in Fig. 1(*b*)) can be expressed as

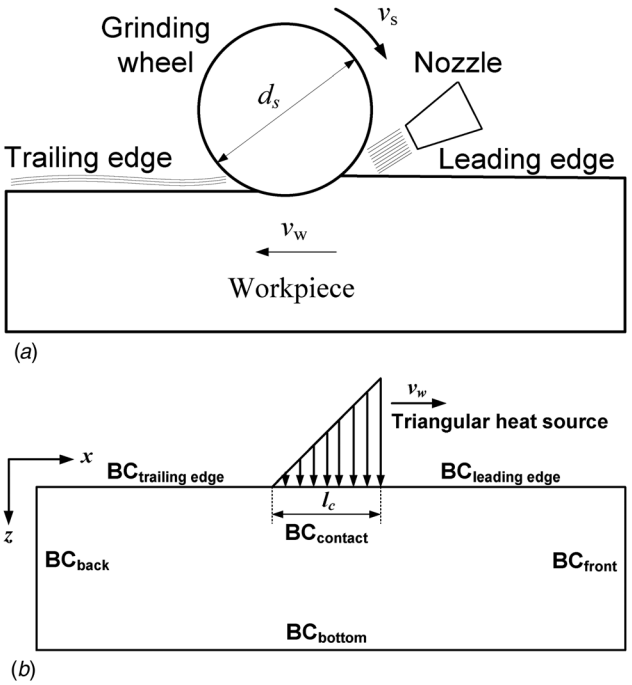

Fig. 2 Illustration of the boundary conditions: (*a*) surface grinding process and (*b*) the corresponding BCs

$$\frac{T_{m+1,n}(t) + T_{m-1,n}(t) - 2T_{m,n}(t)}{(\Delta x)^2} + \frac{T_{m,n+1}(t) + T_{m,n-1}(t) - 2T_{m,n}(t)}{(\Delta z)^2} = \frac{1}{\alpha}\frac{T_{m,n}(t+\Delta t) - T_{m,n}(t)}{\Delta t} \tag{2}$$

Considering the uniform mesh ($\Delta x = \Delta z$), Eq. (1) can be rearranged as following:

$$T_{m,n}(t+\Delta t) = \frac{\alpha \Delta t}{(\Delta x)^2}\left[T_{m-1,n}(t) + T_{m+1,n}(t) + T_{m,n-1}(t) + T_{m,n+1}(t)\right] + \left[1 - 4\frac{\alpha \Delta t}{(\Delta x)^2}\right] T_{m,n}(t) \tag{3}$$

2.2 Boundary Conditions. In FDM, either the full grid or half grid can be used at the boundary. The half grid has the advantage of direct expression of the boundary node temperature, while the full grid requires less computation time. In this study, the full grid at the boundary was adopted. The surface grinding configuration is shown in Fig. 2(*a*). As seen in Fig. 2(*b*), six

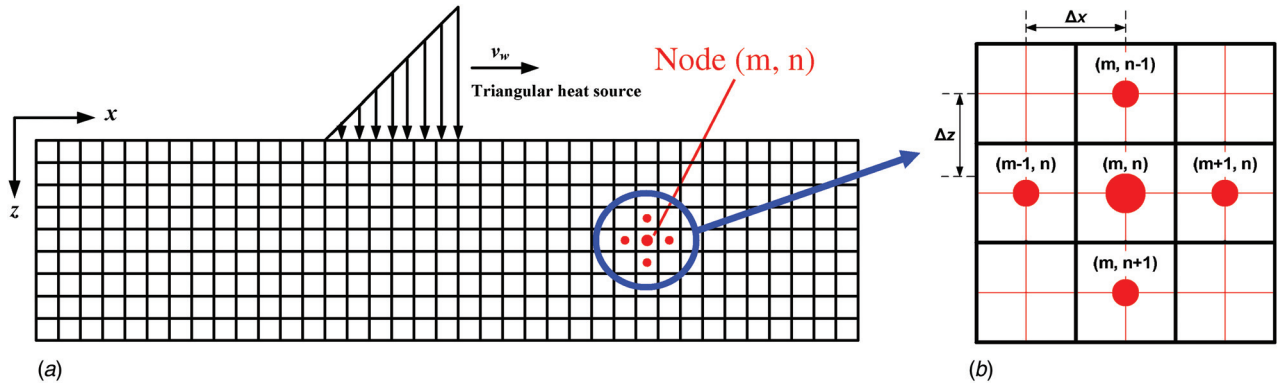

Fig. 1 Illustration of nodal network: (*a*) mesh of the computation domain (workpiece) and (*b*) close-up view of the nodal network

Downloaded 07 Aug 2011 to 141.212.213.57. Redistribution subject to ASME license or copyright; see http://www.asme.org/terms/Terms_Use.cfm

Table 1 Summary of the parameters used in the simulation

Wheel diameter, d_s	177.8 mm
Depth of cut, a	10 μm
Wheel speed, v_s	30 m/s
Feed rate, v_w	2400 mm/min
Thermal conductivity of workpiece, k_w	63 W/m-K
Thermal diffusivity of workpiece, α_w	16.3×10^{-6} m^2/s
Average heat flux	40 W/mm^2

boundaries, the leading edge ($BC_{leading_edge}$), grinding contact zone ($BC_{contact}$), trailing edge ($BC_{trailing_edge}$), front (BC_{front}), back (BC_{back}), and bottom (BC_{bottom}) side of the workpiece need to be considered. Finite difference equations for these boundary conditions (BCs) can be derived by energy conservation and the derived equations are summarized in Appendix A.

2.3 Surface Temperature. Since the full grid was used at the boundary, the temperature on the ground workpiece surface, T^s, needs to be derived using the energy balance method. Finite difference equations for the top surface temperature prediction are presented in Appendix B.

3 Validation of Finite Difference Thermal Model

The FDM heat transfer model can calculate the evolution of temperature within the workpiece which makes it capable to handle the transient heat transfer problems in grinding. To validate the FDM heat transfer model developed in this study, the results of the FDM model are compared with the solution of the traditional heat transfer model [21,23,24].

The FDM heat transfer model was first applied to simulate the spatial and temporal temperature distribution of grinding Dura-Bar 100-70-02 ductile iron workpiece (with length $L = 50$ mm and thickness $H = 10$ mm), which is the commonly used camshaft material in automotive industry. The grinding parameters and workmaterial properties are listed in Table 1. The triangular moving heat source, as shown in Fig. 2(*b*), with an average heat flux of 40 W/mm^2 and a width of contact length $l_c = 1.33$ mm was used. All

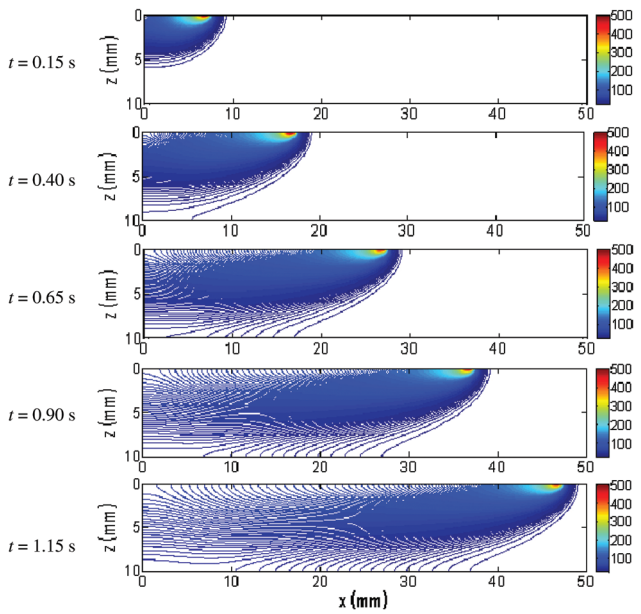

Fig. 3 Temporal and spatial distributions of the workpiece temperature ($L = 50$ mm and $H = 10$ mm)

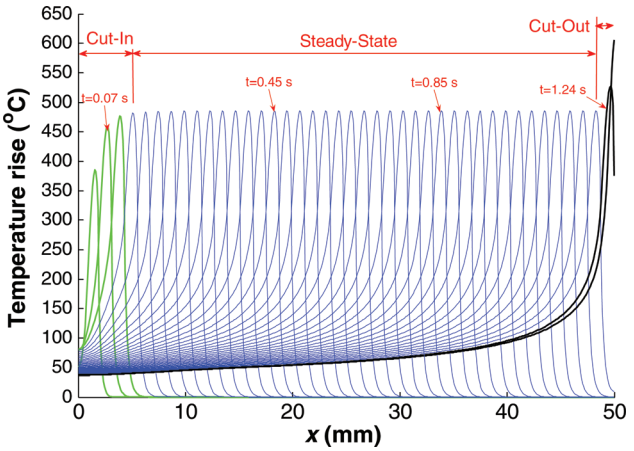

Fig. 4 Temporal and spatial distribution of the grinding temperature at the workpiece surface ($L = 50$ mm, $H = 10$ mm, and $v_w = 2400$ mm/min)

the other BCs are set to be adiabatic, identical to the assumption for the traditional heat transfer model.

The spatial distributions of temperature field in the workpiece at time $t = 0.15$, 0.40, 0.65, 0.90, and 1.15 s are shown in Fig. 3. The time $t = 0$ s is defined at the start of wheel contacting the workpiece. A similar pattern of the temperature field with high temperature region of about 480°C is observed beneath the moving heat source and propagating along the x-axis.

The temporal and spatial distributions of temperature on the ground surface are plotted in Fig. 4. There are three regions, cut-in, steady-state, and cut-out. In the cut-in region, the workpiece peak temperature rises rapidly when the grinding wheel first engages with the workpiece. In the steady-state region, the workpiece surface temperature profile reaches a stable status. The peak temperature maintains at about 480°C, the same level of peak temperature as shown in Fig. 3. As the wheel disengages from the workpiece, due to the boundary condition, the peak temperature increases to 550°C and higher for a short period of time in the cut-out region. The transient heat transfer during the cut-in and cut-out regions has been previously studied by Guo and Malkin [28]. This simulation results also indicate that a steady-state region exists if the workpiece is long enough.

The steady-state FDM heat transfer solution is compared with that of the traditional heat transfer model. As shown in Fig. 5, the FDM surface temperature profile at $t = 0.625$ s (steady-state region) is plotted against the results from the traditional heat transfer model [21,23,24]. The x-axis is the dimensionless distance, x/l, where x is the local coordinate with original point at the

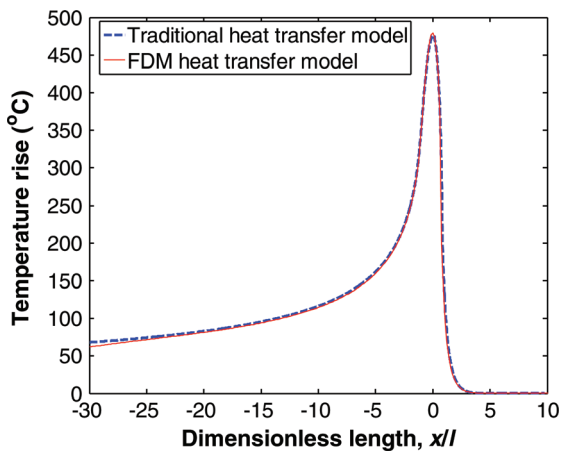

Fig. 5 Comparison of steady-state surface temperature profile

Downloaded 07 Aug 2011 to 141.212.213.57. Redistribution subject to ASME license or copyright; see http://www.asme.org/terms/Terms_Use.cfm

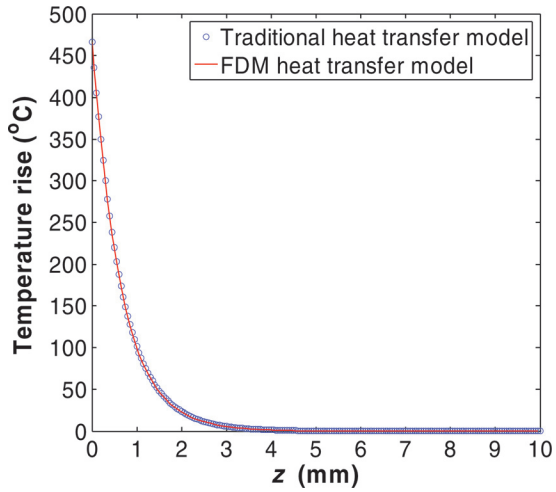

Fig. 6 Comparison of temperature rise along the *z*-direction (at $x/l = 0$)

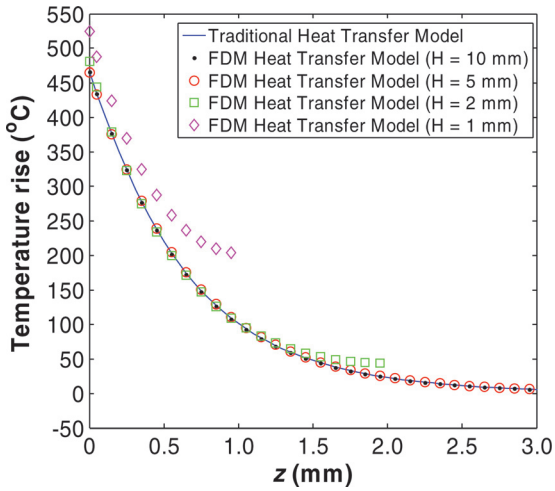

Fig. 8 Effect of the workpiece thickness ($L = 50$ mm and $v_w = 2400$ mm/min)

center of the grinding contact zone and $l = l_c/2$. The results match very well except for a small deviation (less than 10°C) at the far trailing edge ($x/l < -25$). This discrepancy is because the FDM model uses a workpiece with a finite dimension, while the traditional model has an assumption of semiinfinite body.

The temperature rise in the z-direction is also compared. As shown in Fig. 6, very good match of the FDM and traditional heat transfer model results with less than 5 °C discrepancy is observed. This further validates the FDM heat transfer model developed in this study.

4 Effects of Workpiece Dimension and Workpiece Velocity

The effects of workpiece dimensions (length and thickness) are investigated in this section. All the boundary conditions are set to be adiabatic except for the moving heat source in the grinding contact zone, and all the parameters used are listed in Table 1 unless otherwise specified.

4.1 Effect of Workpiece Length. As discussed in Sec. 3, when the workpiece is long, a steady-state region exists. However, if the workpiece is short, the whole process would become a transient heat transfer problem. An example when the length of the workpiece (L) is shortened (from 50 mm as in Sec. 3) to 5 mm (with same thickness $H = 10$ mm) is shown in Fig. 7. The peak temperature at the workpiece surface continues to rise until the grinding wheel disengages with the workpiece. No steady-state can be reached during the whole process.

4.2 Effect of Workpiece Thickness. The thickness of the workpiece mainly affects the temperature rise along the z-direction in the workpiece. The distribution of steady-state grinding surface temperature in the z-direction for $H = 1$, 2, 5, and 10 mm and $L = 50$ mm are shown in Fig. 8. The temperature profile of thick workpiece ($H = 5$ and 10 mm) is almost identical to the traditional heat transfer model which assumes semiinfinite workpiece size. However, the discrepancy starts to show when $H \leq 2$ mm. Also, the thinner workpiece has higher surface temperature because the heat cannot be dissipated in the z-direction.

4.3 Effect of Workpiece Velocity. The workpiece velocity (feed rate) v_w has similar effect as the length of the workpiece because both parameters affect the time scale of heat transfer. For example, as shown in Fig. 9, under the same workpiece size ($L = 50$ mm and $H = 10$ mm), when v_w is small ($v_w = 240$ mm/min), the transient heat transfer becomes dominant and the peak surface temperature continues to rise during the whole grinding process. The overall temperature is also much higher compared to

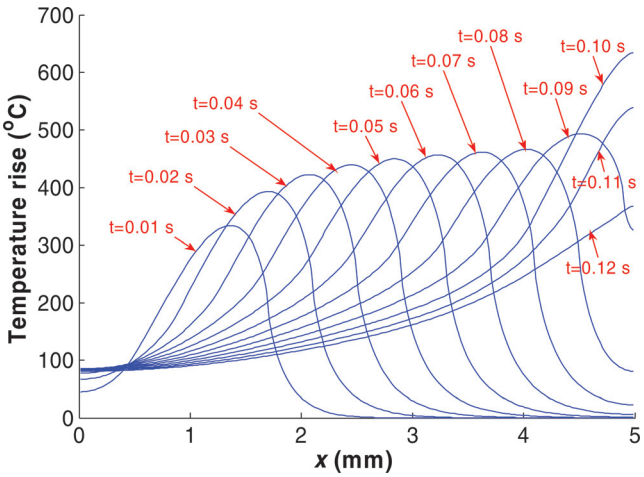

Fig. 7 Effect of the workpiece length ($L = 5$ mm, $H = 10$ mm, and $v_w = 2400$ mm/min)

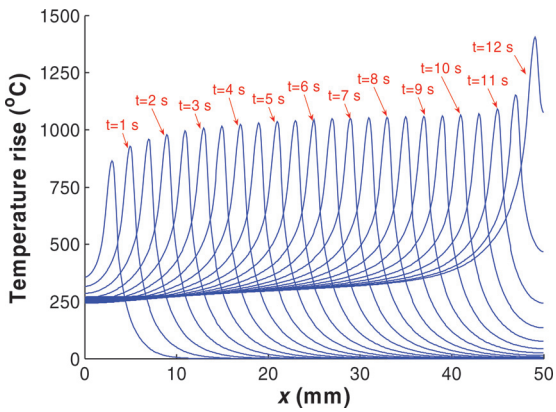

Fig. 9 Effect of the workpiece velocity ($L = 50$ mm, $H = 10$ mm, and $v_w = 240$ mm/min)

Downloaded 07 Aug 2011 to 141.212.213.57. Redistribution subject to ASME license or copyright; see http://www.asme.org/terms/Terms_Use.cfm

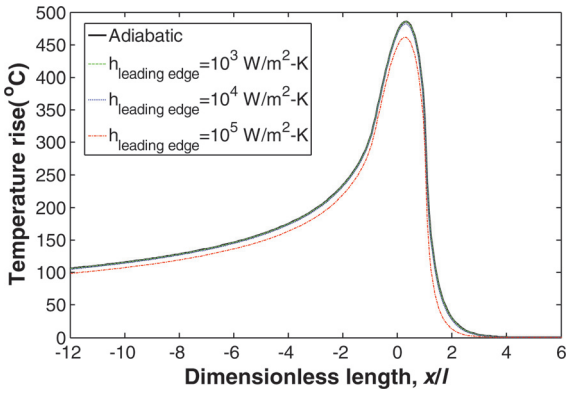

Fig. 10 Effect of cooling in the leading edge (surface temperature)

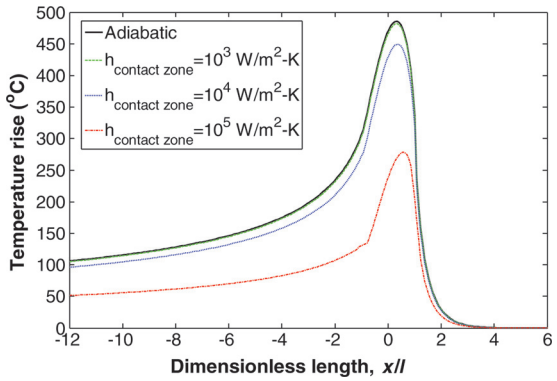

Fig. 12 Effect of cooling in the contact zone (surface temperature)

the results of the workpiece with the same size (Fig. 4) due to the prolonged period for heat conduction.

5 Cooling (Boundary Condition) Effects

An advantage of the FDM grinding heat transfer model is the capability to study the impact of different convective cooling conditions in the leading edge, grinding contact zone, and trailing edge. The adiabatic surface boundary condition (except for the heat flux in the grinding contact zone) is assumed in the traditional heat transfer model. In real life, the boundary conditions can be very complicated, especially when the cutting fluid is applied. In this study, cooling in the three regions (leading edge, grinding contact zone, and trailing edge) are analyzed and discussed.

The range of convection heat transfer coefficient (h) for free convection is from 10 to 10^3 W/m^2-K, while for forced convection and convection with phase change ranges from 10^2 to 10^5 W/m^2-K [34]. Jin et al. [35] reported that the h within the grinding contact zone can be very high, about 2,90,000 W/m^2-K for the water-based cutting fluid and 23 000 W/m^2-K for oil-based cutting fluid. In this study, h is assumed to range from 10^3 to 10^5 W/m^2-K for forced convection and convection with phase change. All the other parameters used in this section are the same as in Table 1.

5.1 Leading Edge. Assuming there is no convection cooling in the grinding contact zone and the trailing edge, while the leading edge has h of 10^3, 10^4, and 10^5 W/m^2-K, the steady-state surface temperature profile is shown in Fig. 10. The effect of cooling in leading edge is minimal. Under high cooling rate with $h = 10^5$W/m^2-K in the leading edge, the peak temperature is reduced by only about 5%.

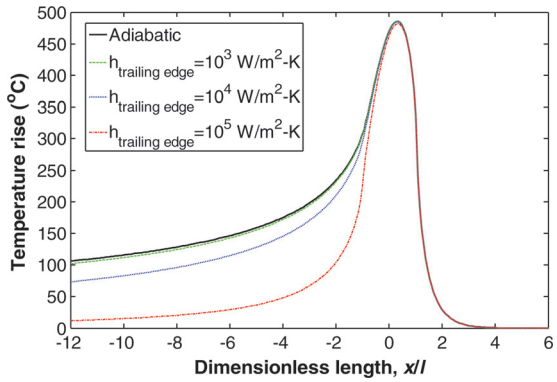

Fig. 11 Effect of cooling in the trailing edge (surface temperature)

5.2 Trailing Edge. By imposing $h = 10^3$, 10^4, and 10^5 W/m^2-K in the trailing edge and assuming there is no convection cooling in the leading edge and grinding contact zone, the steady-state workpiece surface temperature profiles are shown in Fig. 11. Cooling in the trailing edge has a significant impact on the temperature profile. But it only influences the trailing edge, not the grinding contact zone or the leading edge. The peak temperature remains about the same as that in the case of cooling in the leading edge.

5.3 Grinding Contact Zone. For $h = 10^3$, 10^4, and 10^5 W/m^2-K in the grinding contact zone and assuming there is no convection cooling in the leading and trailing edges, the corresponding steady-state workpiece surface temperature profile is shown in Fig. 12. Efficient cooling in the grinding contact zone has a significant impact on the peak temperature and trailing edge temperature. This observation confirms that cooling in the grinding contact zone is critical in the reduction of peak grinding temperature.

6 Application

In this section, the FDM heat transfer model is used to estimate the energy partition and convection heat transfer coefficient in CBN grinding of cast iron under different cooling conditions.

6.1 Experimental Setup. Experiments of straight surface grinding without crossfeed were conducted on an instrumented Chevalier Model Smart-B818 surface grinding machine with 1.5 kW spindle power. The experimental setup is shown in Fig. 13(*a*). The vitrified bond CBN grinding wheel (Universal Abrasive VB126-J160-VT2W19) is about 177.8 mm in diameter and 12.7 mm in width. The surface speed of the wheel (v_s), the feed rate (v_w), and the depth of cut (a) were set at 30 m/s, 2400 mm/min, and 25 μm, respectively. The work-material was Dura-Bar 100-70-02 ductile iron with 63 W/m-K thermal conductivity (k_w) and 1.63×10^{-7} m^2/s thermal diffusivity (α_w). The workpiece was 57 mm in length along the grinding direction and 6.5 mm in width.

Grinding experiments were conducted under dry, wet, and MQL conditions. For wet grinding, the water-based Cimtech 500 synthetic grinding fluid at 5 vol. % was used. MQL grinding, as shown in Fig. 13(*b*), utilized a special fluid application device provided by AMCOL (Hazel Park, MI). The soybean oil was used for MQL application. The flow rate was 5400 ml/min for wet grinding and 5 ml/min for MQL grinding.

Downloaded 07 Aug 2011 to 141.212.213.57. Redistribution subject to ASME license or copyright; see http://www.asme.org/terms/Terms_Use.cfm

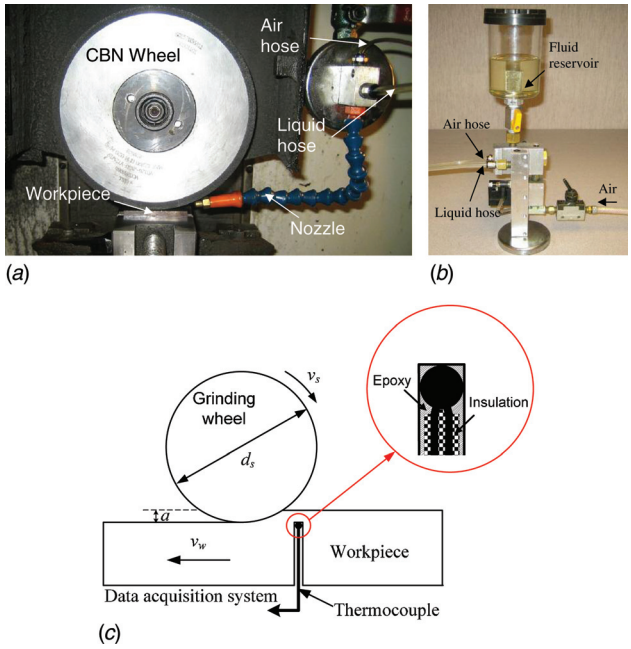

Fig. 13 Experimental setup: (*a*) overview, (*b*) MQL fluid delivery device, and (*c*) illustration of grinding temperature measurement

The normal and tangential grinding forces were measured using a Kistler Model 9257A piezoelectric dynamometer. The workpiece grinding temperatures were measured by the embedded thermocouple method—with an epoxied thermocouple [36] in a blind hole as shown in Fig. 13(*c*). In this method, the epoxy is used to affix the embedded tip of a thermocouple to the end of a blind hole inside the workpiece. During grinding, the thermocouple junction is exposed and bonded to the workpiece by smearing of the work-material, thereby providing a direct contact and measurement of temperature at the workpiece surface. The temperature and grinding force data were collected at a sampling rate of 5 kHz. After each grinding pass, the workpiece was allowed to cool to the initial temperature before the next pass was taken.

6.2 Energy Partition Prediction. In grinding, heat is generated through friction and plastic deformation at three locations: grain-workpiece interface, grain-chip interface, and workpiece-chip shear plane. For simplicity, the heat will be thought of as being generated at grain-workpiece interface [16], and this heat instantaneously conducts into the workpiece and the wheel. Once the heat enters the workpiece, it may either remain in the workpiece ($q_{workpiece}$) or be removed by convection to the cutting fluid ($q_{f\text{-}w}$) [17–19], and similarly the heat which conducts into the grinding wheel may either remain in the grinding wheel (q_{wheel}) or partially be removed by the cutting fluid ($q_{f\text{-}g}$). According to Lavine and Jen [16], the heat transferred from the grain to the fluid is not very significant, and in this study, the heat transferred from the workpiece to the fluid ($q_{f\text{-}w}$) is of the most interest.

The energy partition is defined as the fraction of the heat entering the workpiece. The FDM heat transfer model solves the temporal distribution of the temperature in the workpiece, rather than giving just a steady-state solution. Therefore, the temperature response measured by the thermocouple, which is in the time domain, can be directly matched to the results calculated from the FDM heat transfer model.

Given the total heat generated in the grinding contact zone (q_{total}), to calculate the energy partition it is necessary to find the heat flux into the workpiece, which is assumed to have a triangular distribution over the grinding contact length l_c. The q_{total} is assumed to be partitioned among the grinding wheel (q_{wheel}), the workpiece ($q_{workpiece}$), and the cutting fluid ($q_{f\text{-}w} + q_{f\text{-}g}$)

$$q_{total} = (q_{wheel} + q_{f-g}) + (q_{workpiece} + q_{f-w}) = \frac{F_t v_s}{b_w l_c} \tag{4}$$

where F_t is the tangential grinding force and b_w is the width of the workpiece or the wheel, whichever is less.

In dry grinding, there is no heat carried away by the cutting fluids; therefore

$$q_{total} = q_{wheel} + q_{workpiece} = q_{wheel} + \varepsilon_{dry} q_{total} \tag{5}$$

where $\varepsilon_{dry} = q_{workpiece}/q_{total}$ is the energy partition into the workpiece under dry condition.

In wet and MQL grinding, the heat also enters into the cutting fluid, thus

$$\begin{aligned} q_{total} &= (q_{wheel} + q_{f-g}) + (q_{workpiece} + q_{f-w}) = q_{whf} + q_{wf} \\ q_{whf} &= q_{wheel} + q_{f-g} \\ q_{wf} &= q_{workpiece} + q_{f-w} = \varepsilon_{wf} q_{total} = \varepsilon_w q_{total} + q_{f-w} \end{aligned} \tag{6}$$

where q_{whf} is the heat remaining in the wheel plus the heat entering the fluid through wheel-fluid interaction, q_{wf} is the heat remaining in the workpiece plus the heat entering the fluid through workpiece-fluid interaction, $\varepsilon_{wf} = q_{wf}/q_{total}$ and $\varepsilon_w = q_{workpiece}/q_{total}$ are the energy partition into the workpiece (before and after the heat enters the fluid) under the wet/MQL condition.

The energy partition in dry, wet or MQL grinding can be solved using the temperature matching method [21]. In this method, by adjusting the $q_{workpiece}$, the predicted surface temperature profile is matched to the measured temperature using least square method (finding the least square error between the predicted and measured temperature profiles). Once the $q_{workpiece}$ is found, the energy partition into the workpiece can be determined (ε_{dry} or $\varepsilon_w = q_{workpiece}/q_{total}$). The energy partition values in Table 2 [37] were estimated by temperature matching method using the traditional heat transfer model [21]. The same results with less than 0.1% discrepancy can also be obtained using the proposed FDM heat transfer model by imposing the adiabatic BCs on all the workpiece surfaces except in the grinding contact zone, as shown in Fig. 14. The only difference is that the temperature matching was done in the time domain instead of in the space domain. The

Table 2 Grinding parameters and corresponding energy partition results [37]

Cutting fluid application	Flow rate (ml/min)	Depth of cut (μm)	Feed rate (mm/min)	Energy partition (ε_{dry} or ε_w)
Dry	–	25	2400	68.7%
MQL (soybean oil)	5			53.8%
Wet (5 vol. % Cimtech 500 synthetic grinding fluid)	5400			13.2%

Downloaded 07 Aug 2011 to 141.212.213.57. Redistribution subject to ASME license or copyright; see http://www.asme.org/terms/Terms_Use.cfm

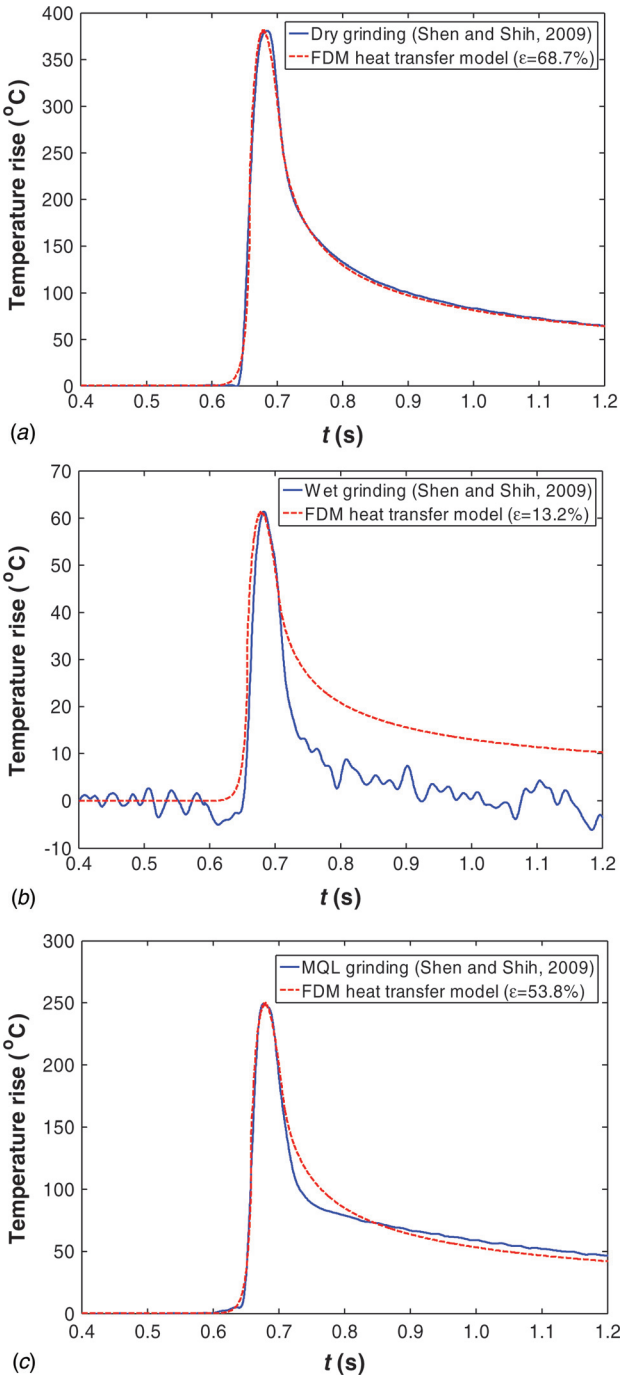

Fig. 14 Temperature matching results: (*a*) dry grinding, (*b*) wet grinding, and (*c*) MQL grinding

energy partition into the workpiece is 69% for dry grinding, 54% for MQL grinding, and 13% for wet grinding. The reduced energy partition values in MQL and wet grinding are attributed to the convection cooling at the workpiece surface ($q_{f\text{-}w}$).

In Figs. 14(*b*) and 14(*c*), the deviation from the experimental measurements and FDM results is evident under the wet and MQL conditions due to the assumption of adiabatic BCs in the leading edge and trailing edge. This problem can be solved by using the appropriate boundary conditions. The FDM heat transfer model is further developed in Sec. 6.3 to estimate the convection heat transfer coefficient in the grinding process.

6.3 Convection Heat Transfer Coefficient Prediction. The FDM heat transfer model can be used to estimate the convection

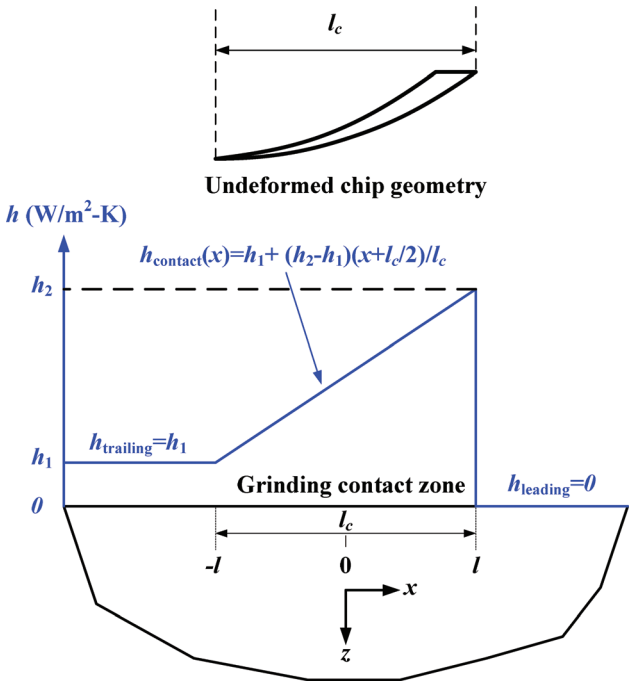

Fig. 15 Assumption of convection heat transfer coefficient

heat transfer coefficient at the workpiece surface in the critical grinding contact zone and the trailing edge. The convection heat transfer coefficient instead of the $q_{\text{workpiece}}$ is the variable adjusted to minimize the discrepancy between the FDM predicted and experimentally measured surface temperature. Therefore, in this case the heat flux q_{wf} (the heat remaining in the workpiece plus the heat enters the fluid through workpiece-fluid interaction) becomes the input for the FDM model. In order to estimate the heat flux q_{wf} from the experiment, an assumption was made for this model: the energy partition ratio between the workpiece and the grinding wheel in dry condition remains the same as in wet and MQL condition before the heat was transferred to the cutting fluid, meaning that $q_{\text{workpiece}}/q_{\text{wheel}} = q_{\text{wf}}/q_{\text{whf}}$. Based on this assumption, $\varepsilon_{\text{dry}} = \varepsilon_{\text{wf}}$ and $q_{\text{wf}} = \varepsilon_{\text{wf}} q_{\text{total}} = \varepsilon_{\text{dry}} q_{\text{total}}$ for wet and MQL grinding. Thus, as long as ε_{dry} is known, the heat flux input q_{wf} for the FDM heat transfer model can be found. This assumption may not be perfect; however, it is the first step to enable the analysis, and it can be further improved by establishing better assumptions in the future research.

For wet and MQL grinding, the heat flux into the fluid through workpiece-fluid interaction can be expressed as

$$q_{f-w} = \int_{-l}^{l} h(x)[T^s(x) - T_a]dx \tag{7}$$

where T_a is the fluid (or ambient) temperature.

The actual depth of cut in the grinding contact zone decreases from the leading edge side to the trailing edge side for down grinding. This creates the nonuniform flow channel, leading to nonuniform convective cooling. As shown in Fig. 15, the convection heat transfer coefficient in the grinding contact zone, h_{contact}, is assumed as a linear function.

$$h_{\text{contact}}(x) = h_1 + \frac{h_2 - h_1}{l_c}\left(x + \frac{l_c}{2}\right) \tag{8}$$

where $h_2 = \max[h_{\text{contact}}(x)], h_1 = \min[h_{\text{contact}}(x)]$, and x is the local coordinate with original point at the center of the grinding contact

Downloaded 07 Aug 2011 to 141.212.213.57. Redistribution subject to ASME license or copyright; see http://www.asme.org/terms/Terms_Use.cfm

zone. The average convection heat transfer coefficient in the grinding contact zone, $\overline{h}_{\text{contact}}$, is defined as

$$\overline{h}_{\text{contact}} = \frac{h_1 + h_2}{2} \tag{9}$$

The convection heat transfer coefficient in the trailing edge, h_{trailing}, is assumed to be uniform. At $x = -l$, the convection heat transfer coefficient is assumed to be the same at the trailing edge as at the end of the grinding contact zone, where the actual depth of cut is close to zero. Therefore

$$h_{\text{trailing}} = h_1 \tag{10}$$

According to Sec. 5, cooling effect in the leading edge is negligible. Hence $\text{BC}_{\text{leading_edge}}$ is set to be adiabatic. The other three boundaries, BC_{back}, BC_{front}, and $\text{BC}_{\text{bottom}}$, are all set to be adiabatic. A triangular heat source with an average heat flux of $q_{\text{wf}}/b_w l_c$ is used.

By matching the measured temperature profile to the calculated temperature from the FDM heat transfer model, the convection heat transfer coefficient in the grinding contact zone ($\overline{h}_{\text{contact}}$) and in the trailing edge (h_{trailing}) can be solved. The temperature matching results are shown in Fig. 16. The estimated convection heat transfer coefficient values for wet and MQL grinding are summarized in Table 3. The convection heat transfer coefficient

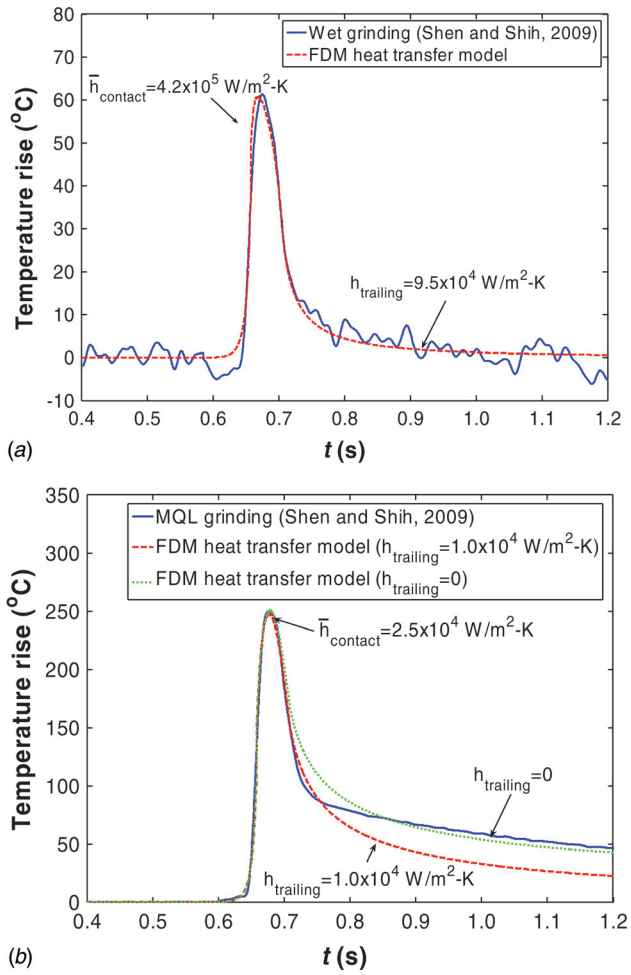

Fig. 16 Convection heat transfer coefficient prediction: (*a*) wet grinding and (*b*) MQL grinding

Table 3 Predicted convection heat transfer coefficient

Cutting fluid application	h_2 (W/m^2-K)	$\overline{h}_{\text{contact}}$ (W/m^2-K)	h_{trailing} (W/m^2-K)
MQL (soybean oil)	3.9×10^4	2.5×10^4	1.0×10^4
Wet (5 vol. % Cimtech 500 synthetic grinding fluid)	7.4×10^5	4.2×10^5	9.5×10^4

in the grinding contact zone is much higher than that in the trailing edge for both cases. This is expected because of the much higher fluid velocity in the grinding contact zone. Wet grinding has much higher convection heat transfer coefficient than MQL grinding both in the grinding contact zone and the trailing edge.

Compared to Fig. 14(*b*), the wet grinding temperature profile with the linearly varying convection heat transfer coefficient in the grinding contact zone as shown in Fig. 16(*a*) gives a very good matching between the FDM predicted and experimentally measured temperature profiles, especially in the trailing edge. For MQL grinding, as seen in Fig. 16(*b*), the matching of temperature profiles in the trailing edge is not ideal. This indicates that the convection heat transfer coefficient in the trailing edge may not be uniform under MQL condition. The calculated temperature profile with a high h_{trailing} matches with experimental measurements very well in the trailing edge near the grinding contact zone, but not in the trailing edge away from the grinding contact zone. The calculated temperature profile with a zero h_{trailing} has a better match in the trailing edge away from the grinding contact zone. This is because MQL only provided some cooling in the trailing edge near the grinding contact zone and the convection heat transfer is very poor in trailing edge region further away from the grinding zone due to the low MQL flow rate (the cutting fluid may not completed cover the workpiece-wide trailing edge as observed). Therefore, the actual convection heat transfer in the trailing edge for MQL grinding is also nonuniform and needs further study.

7 Conclusions

A FDM based heat transfer model for grinding, which is more capable and flexible when dealing with transient heat transfer and different boundary conditions, was developed and validated by comparing with the traditional heat transfer model. The FDM heat transfer model was used to study effects of workpiece size, workpiece velocity (feed rate), and cooling in the leading edge, trailing edge and grinding contact zone. Simulations results showed that transient heat transfer occurred in the cut-in and cut-out regions even though the steady-state can be reached during the process, and when the workpiece was short or the feed rate was low, the transient heat transfer effect was more significant. Results also showed that the thickness of the workpiece could influence the temperature profile along the z-direction in the workpiece. In addition, from the simulation results it was concluded that cooling in the leading edge was insignificant; cooling in the trailing edge helped to cool the workpiece but could not reduce the peak temperature; and the most efficient cooling occurred in the grinding contact zone.

The FDM heat transfer model was further applied in the grinding experiments to estimate the energy partition and the convection heat transfer coefficient. Due to the fact that the actual depth of cut in the grinding contact zone decreases from the leading edge to the trailing edge for down grinding, which forms a nonuniform flow channel, an assumption of linearly varying convection heat transfer coefficient in the grinding contact zone has been proposed. Based on this assumption, the estimated average convection heat transfer coefficient in the experiment is 4.2×10^5 W/m^2-K for wet grinding and 2.5×10^4 W/m^2-K for MQL grinding.

Downloaded 07 Aug 2011 to 141.212.213.57. Redistribution subject to ASME license or copyright; see http://www.asme.org/terms/Terms_Use.cfm

Acknowledgment

This research was sponsored by National Science Foundation DMII Grant No. #0422947 and General Motors Research. Support from Saint-Gobain and AMCOL Corporation are greatly appreciated. The authors also thank Professor Stephen Malkin and Dr. Changsheng Guo (United Technology Research Center) for their discussion and advice.

Appendix A: Boundary Conditions

For the boundary condition in the grinding contact zone, as shown in Fig. 17, by considering the heat conduction between the nodes, heat flux from the wheel-workpiece interface, as well as the forced convection or convection with phase change within the grinding contact zone, the energy conservation gives

$$q_{(m-1,1)\to(m,1)} + q_{(m+1,1)\to(m,1)} + q_{(m,2)\to(m,1)} + q''A = \rho c_p V_o \frac{\partial T}{\partial t} + G_{\text{contact}} A\left[T_{m,1}(t) - T_a\right] \tag{A1}$$

where ρ is density, C_p is the specific heat capacity of workpiece, T_a is the fluid (or ambient) temperature, $T_{m,1}$ is the temperature at the node $(m,1)$, and q'' is the heat flux into the surface boundary. Assuming the depth is equal to the unit length, $V_o = \Delta x \Delta z$ is the volume of the grid and $A = \Delta x$ is the surface area of the boundary between the grids. G_{contact} is the combined heat transfer coefficient, defined as

$$G_{\text{contact}} = \left(\frac{1}{h_{\text{contact}}} + \frac{\Delta z}{2k}\right)^{-1} \tag{A2}$$

where h_{contact} is the convection heat transfer coefficient in the contact zone and k is the thermal conductivity of the workpiece. The heat flux terms in Equation (A1) can be expressed as

$$q_{(m-1,1)\to(m,1)} = k\Delta z\left[\frac{T_{m-1,1}(t) - T_{m,1}(t)}{\Delta x}\right] \tag{A3}$$

$$q_{(m+1,1)\to(m,1)} = k\Delta z\left[\frac{T_{m+1,1}(t) - T_{m,1}(t)}{\Delta x}\right] \tag{A4}$$

$$q_{(m,2)\to(m,1)} = k\Delta x\left[\frac{T_{m,2}(t) - T_{m,1}(t)}{\Delta z}\right] \tag{A5}$$

where $T_{m-1,1}$, $T_{m+1,1}$, $T_{m,2}$ are the temperatures at the adjacent nodes.

Equation (A1) can be rewritten as

$$T_{m,1}(t+\Delta t) = \frac{(\Delta x)^2}{\alpha \Delta t}\left[T_{m-1,1}(t) + T_{m+1,1}(t) + T_{m,2}(t) + \frac{G_{\text{contact}}\Delta x}{k} T_a\right] + \left[1 - 3\frac{(\Delta x)^2}{\alpha \Delta t} - \frac{(\Delta x)^2}{\alpha \Delta t}\frac{G_{\text{contact}}\Delta x}{k}\right] T_{m,1}(t) + \frac{(\Delta x)^2}{\alpha \Delta t}\frac{q''\Delta x}{k} \tag{A6}$$

For the BC in the leading edge, there is no heat flux; therefore, the $\text{BC}_{\text{leading_edge}}$ can be derived by modifying Eq. (A6)

$$T_{m,1}(t+\Delta t) = \frac{(\Delta x)^2}{\alpha \Delta t}\left[T_{m-1,1}(t) + T_{m+1,1}(t) + T_{m,2}(t) + \frac{G_{\text{leading}}\Delta x}{k} T_a\right] + \left[1 - 3\frac{(\Delta x)^2}{\alpha \Delta t} - \frac{(\Delta x)^2}{\alpha \Delta t}\frac{G_{\text{leading}}\Delta x}{k}\right] T_{m,1}(t) \tag{A7}$$

where

$$G_{\text{leading}} = \left(\frac{1}{h_{\text{leading}}} + \frac{\Delta z}{2k}\right)^{-1}$$

and h_{leading} is the convection heat transfer coefficient in the leading edge.

All the other boundary conditions ($\text{BC}_{\text{trailing_edge}}$, BC_{back}, BC_{front}, and $\text{BC}_{\text{bottom}}$) are very similar to Eq. (A7). Note that, if the adiabatic boundary is imposed, all the BCs will still hold by simply setting the convection heat transfer coefficient (h_{contact}, h_{leading}, h_{trailing}, h_{front}, or h_{back}) to zero.

Appendix B: Surface Temperature

As seen in Fig. 18, the energy conversation at the surface (within the contact zone) gives (assuming the depth is equal to the unit length)

$$q''A = q_{\text{surface}\to(m,1)} + h_{\text{contact}} A\left[T^s_{m,1}(t) - T_a\right] \tag{B1}$$

$$q''\Delta x = k\Delta x\left[\frac{T^s_{m,1}(t) - T_{m,1}(t)}{\Delta z/2}\right] + h_{\text{contact}}\Delta x\left[T^s_{m,1}(t) - T_a\right] \tag{B2}$$

$$T^s_{m,1}(t) = \frac{q''\Delta z/k + 2T_{m,1}(t) + h_{\text{contact}}\Delta z T_a/k}{(2 + h_{\text{contact}}\Delta z/k)} \tag{B3}$$

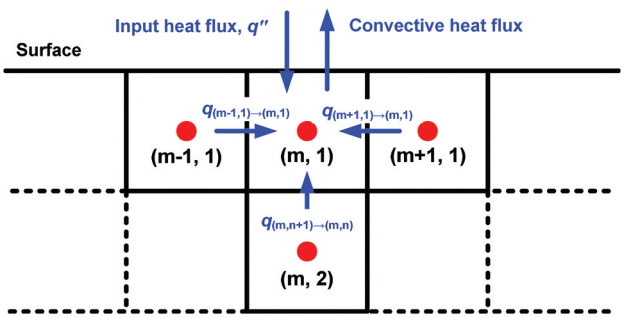

Fig. 17 BC within the contact zone

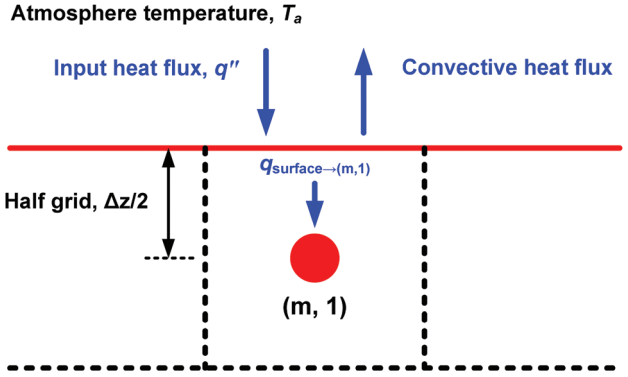

Fig. 18 Interpretation of the surface temperature (contact zone)

Downloaded 07 Aug 2011 to 141.212.213.57. Redistribution subject to ASME license or copyright; see http://www.asme.org/terms/Terms_Use.cfm

where $T^s_{m,1}$ is the interpreted surface temperature next to the node $(m,1)$.

Similarly, the surface temperature in the region of leading and trailing edges can be expressed as following, respectively.

$$T^s_{m,1}(t) = \frac{2T_{m,1}(t) + h_{\text{leading}}\Delta z T_a/k}{\left(2 + h_{\text{leading}}\Delta z/k\right)} \tag{B4}$$

$$T^s_{m,1}(t) = \frac{2T_{m,1}(t) + h_{\text{trailing}}\Delta z T_a/k_a}{\left(2 + h_{\text{trailing}}\Delta z/k\right)} \tag{B5}$$

References

[1] Malkin, S., 1989, *Grinding Technology: Theory and Applications of Machining With Abrasives*, John Wiley & Sons, New York.

[2] Jaeger, J. C., 1942, "Moving Sources of Heat and the Temperature at Sliding Contacts," J. Proc. R. Soc. N. S. W., **76**, pp. 203–224.

[3] Outwater, J. O., and Shaw, M. C., 1952, "Surface Temperatures in Grinding," Trans. ASME, **74**, pp. 73–86.

[4] Hahn, R. S., 1956, "The Relation Between Grinding Conditions and Thermal Damage in the Workpiece," Trans. ASME, **78**, pp. 807–812.

[5] Snoeys, R., Roesems, D., Vandeurzen, U., and Vanhonacker, P., 1979, "Survey on Modal Analysis Applications," CIRP Ann., **28**(2), pp. 497–510.

[6] Malkin, S., 1984, "Grinding of Metals: Theory and Application," J. Appl. Metalworking, **3**, pp. 95–109.

[7] Takazawa, K., 1972, "Thermal Aspects of the Grinding Operation," Ind. Diamond Rev. **4**, pp. 143–149.

[8] Rowe, W. B., Pettit, J. A., Boyle, A., and Moruzzi, J. L., 1988, "Avoidance of Thermal Damage in Grinding," CIRP Ann., **37** pp. 327–330.

[9] Shaw, M. C., 1990, "A Simplified Approach to Workpiece Temperature in Fine Grinding," CIRP. Ann., **39**, pp. 345–347.

[10] Hahn, R. S., 1962, "On the Nature of the Grinding Process," Proceedings of the 3rd Machine Tool Design and Research Conference, pp. 129–154.

[11] Hahn, R. S., 1966, "On the Mechanics of the Grinding Process Under Plunge Cut Conditions," J. Eng. Ind., **88**, pp. 72–80.

[12] Liao, Y. S., Luo, S. Y., and Yang, T. H., 2000, "Thermal Model of the Wet Grinding Process," J. Mater. Process. Technol., **101**(1), pp. 137–145.

[13] Maksoud, T. M. A., 2005, "Heat Transfer Model for Creep-Feed Grinding," J. Mater. Process. Technol., **168**(3), pp. 448–463.

[14] Rowe, W. B., Black, S. C. E., and Mills, B., 1996, "Temperature Control in CBN Grinding," Int. J. Adv. Manuf. Technol., **12**, pp. 387–392.

[15] Lavine, A. S., 1988, "A Simple Model for Convective Cooling During the Grinding Process," J. Eng. Ind., **110** pp. 1–6.

[16] Lavine, A. S., and Jen, T. C., 1991, "Thermal Aspects of Grinding: Heat Transfer to Workpiece, Wheel, and Fluid," J. Heat Transfer, **113** pp. 296–303.

[17] Lavine, A. S., and Jen, T. C., 1991, "Coupled Heat Transfer to Workpiece, Wheel, and Fluid in Grinding, and the Occurrence of Workpiece Burn," Int. J. Heat Mass Transfer, **34**, pp. 983–992.

[18] Jen, T. C., and Lavine, A. S., 1995, "A Variable Heat Flux Model of Heat Transfer in Grinding: Model Development," J. Heat Transfer, **117**(2), pp. 473–478.

[19] Demetriou, M. D., and Lavine, A. S., 2000, "Thermal Aspects of Grinding: The Case of Upgrinding," J. Manuf. Sci. Eng., **122**(4), pp. 605–611.

[20] Ju, Y., Farris, T. N., and Chandrasekar, S., 1998, "Theoretical Analysis of Heat Partition and Temperatures in Grinding," J. Tribol., **120**(4), pp. 789–794.

[21] Kohli, S. P., Guo, C., and Malkin, S., 1995, "Energy Partition for Grinding With Aluminum Oxide and CBN Abrasive Wheels,"J. Eng. Ind., **117** pp. 160–168.

[22] Guo, C., and Malkin, S., 1995, "Analysis of Energy Partition in Grinding," J. Eng. Ind., **117**, pp. 55–61.

[23] Guo, C., and Malkin, S., 1996, "Inverse Heat Transfer Analysis of Grinding, Part 1: Methods,"J. Eng. Ind., **118** (1) (1996) 137–142.

[24] Guo, C., and Malkin, S., 1996, "Inverse Heat Transfer Analysis of Grinding, Part 2: Applications," J. Eng. Ind., **118**(1), pp. 143–149.

[25] Hong, K. K., and Lo, C. Y., 2000, "Inverse Analysis for the Heat Conduction During a Grinding Process," J. Mater. Process. Technol., **105**(1), pp. 87–94.

[26] Wang, C. C., and Chen, C. K., 2002, "Three-Dimensional Inverse Heat Transfer Analysis During the Grinding Process," J. Mech. Eng. Sci., **216** pp. 199–214.

[27] Kim, H. J., Kim, N. K., and Kwak, J. S., 2006, "Heat Flux Distribution Model by Sequential Algorithm of Inverse Heat Transfer for Determining Workpiece Temperature in Creep Feed Grinding," Int. J. Mach. Tools Manuf., **46**(15), pp. 2086–2093.

[28] Guo, C., and Malkin, S., 1995, "Analysis of Transient Temperatures in Grinding," J. Eng. Ind., **117**, pp. 571–577.

[29] Mahdi, M., and Zhang, L., 1995, "The Finite Element Thermal Analysis of Grinding Processes by ADINA," Comput. Struct., **56**, pp. 313–320.

[30] Biermann, D., and Schneider, M., 1997, "Modeling and Simulation of Workpiece Temperature in Grinding by Finite Element Analysis," Mach. Sci. Technol., **1**(2), pp. 173–183.

[31] Wang, L., Qin, Y., Liu, Z. C., Ge, P. Q., and Gao, W., 2003, "Computer Simulation of a Workpiece Temperature Field During the Grinding Process," Proc. Inst. Mech. Eng., Part B, **217**(7), pp. 953–959.

[32] Mamalis, A. G., Kundrak, J., Manolakos, D. E., Gyani, K., and Markopoulos, A., 2003, "Thermal Modeling of Surface Grinding Using Implicit Finite Element Techniques," Int. J. Adv. Manuf. Technol., **21**(12), pp. 929–934.

[33] Lefebvre, A., Vieville, P., Lipinski, P., and Lescalier, C., 2006, "Numerical Analysis of Grinding Temperature Measurement by the Foil/Workpiece Thermocouple Method," Int. J. Mach. Tools Manuf., **46**(14), pp. 1716–1726.

[34] Incropera, F. P., and DeWitt, D. P., 2001, *Fundamentals of Heat and Mass Transfer*, Wiley, New York.

[35] Jin, T., Stephenson, D. J., and Rowe, W. B., 2001, "Estimation of the Convection Heat Transfer Coefficient of Coolant Within the Grinding Zone," Proc. Inst. Mech. Eng., Part B, **217**, pp. 397–407.

[36] Shen, B., Xiao, G., Guo, C., Malkin, S., and Shih, A. J., 2008, "Thermocouple Fixation Method for Grinding Temperature Measurement," ASME J. Manuf. Sci. Eng., **130**, p. 051014.

[37] Shen, B., and Shih, A. J., 2009, "Minimum Quantity Lubrication (MQL) Grinding Using Vitrified CBN Wheels," Trans. NAMRI/SME, **37**, pp. 129–136.

Downloaded 07 Aug 2011 to 141.212.213.57. Redistribution subject to ASME license or copyright; see http://www.asme.org/terms/Terms_Use.cfm